Electronic Supporting Information (ESI)

Mild and scalable synthesis of high performance CrFeCoNiRu$_{0.5}$ high entropy nano-alloy/carbon electrocatalyst for efficient urea production using chelate-based ionic liquid

Zhang Qingqing[a], Li Ruiyi[a], Li Zaijun[a*], Yang Yongqiang[b] and Liu Xiaohao[a]

[a] Key Laboratory of Synthetic and Biological Colloids, Ministry of Education, School of Chemical and Material Engineering, School of Life Science and Health Engineering, Jiangnan University, Wuxi 214122, China

[b] National Graphene Products Quality Supervision and Inspection Center (Jiangsu), Jiangsu Province Special Equipment Safety Supervision Inspection Institute· Branch of Wuxi, Wuxi 214174, China

1. Experimental

1.1 Prediction of phase formation for the designed CrFeCoNiRu$_{0.5}$

The main factors affecting the formation of solid solution phase of high entropy alloy are atomic radius difference, chemical compatibility between principal components (mixing enthalpy), mixing entropy, valence electron concentration and thermodynamic parameters (Ω)[1-2]. Thermodynamic and geometric parameters of phase formation in CrFeCoNiRu$_{0.5}$ high entropy alloy (HEA) are calculated by Formula (4-9)[3-4].

$$\delta = \sqrt{\sum_{i=1}^{n} c_i (1 - \frac{r_i}{\bar{r}})^2} \times 100\%$$

$$\bar{r} = \sum_{i=1}^{n} c_i r_i \tag{1}$$

$$\Delta H_{mix} = \sum_{i=1, \ i \neq j}^{n} 4 \Delta H_{ij}^{mix} c_i c_j \tag{2}$$

$$\Delta S_{mix} = -R \sum_{i=1}^{n} (c_i \ln c_i) \tag{3}$$

$$T_m = \sum_{i=1}^{n} c_i (T_m)_i \qquad (4)$$

$$\Omega \ (T) = \frac{T\Delta S_{mix}}{\left|\Delta H_{mix}\right|} \qquad (5)$$

$$VEC = \sum_{i=1}^{n} c_i (VEC)_i \qquad (6)$$

Where $\bar{r}$ is the average radius of HEA element atoms; r_i is the atom radius of the ith element; $_{\Delta H_{ij}^{mix}}$ is the enthalpy of mixing of the binary liquid alloy consisting of the ith principal element and the jth principal element; c_i or c_j is the atomic content of the ith principal element or the jth principal element; R is the gas constant; c_i is the atomic content of the ith principal element; T_m is the melting point of HEA; $(T_m)_i$ is the melting point of the ith principal element of HEA; $(VEC)_i$ is the valence electron concentration of the ith principal element in HEA.

Multi-principal HEA tend to form stable solid solution phases when $-11.6 < \Delta H_{mix} \leq 3.2$ kJ·mol^{-1},12 $< \Delta S_{mix} \leq 17.$ 5 J·K^{-1}·mol^{-1},1$<\delta<6.6\%$, $\Omega \geq 1.1$[5-6]. When the valence electron concentration VEC≥ 8.0, HEA is easy to form FCC solid solution phase; When VEC<6.87, HEA is easy to form BCC solid solution phase; When $6.87 \leq$ VEC<8.0, BCC phase coexists with FCC and BCC phase[7]. Table S1 summarizes the binary mixing enthalpy and physical and chemical parameters of CrFeCoNiRu$_{0.5}$. These values are used to calculate the thermodynamic parameters listed in Table S2. The calculated thermodynamic and geometrical parameters listed in Table S2 predict that CrFeCoNiRu$_{0.5}$ will form random solid solution with FCC crystal structures.

1.2 Chemicals and Materials

Iron (III) chloride hexahydrate (FeCl$_3$·6H$_2$O, $\geq 99.0\%$), nickel chloride hexahydrate (NiCl$_2$·6H$_2$O, $\geq 98.0\%$), cobalt chloride hexahydrate (CoCl$_2$·6H$_2$O, $\geq 99.0\%$), ruthenium (III) chloride hydrate (RuCl$_3$·xH$_2$O, 40.0%), chromium (III) chloride hexahydrate (CrCl$_3$·6H$_2$O, $\geq 99.0\%$), citric acid

monohydrate ($C_6H_8O_7 \cdot H_2O$, AR), potassium nitrate (KNO_3, AR), urea (CH_4N_2O, AR), diacetylmonoxime ($C_4H_7NO_2$, AR), thiosemicarbazide (TSC, AR), potassium sulphate (K_2SO_4, AR) were purchased from Sinopharm Chemical Reagent Co. Ltd (Shanghai, China). Nafion117 solution (5 wt%) were purchased from Shanghai Macklin Biochemical Co., Ltd. Ionic liquids are obtained by reported methods [8]. Salicylicacid ($C_7H_6O_3$, AR), octylamine ($C_8H_{19}N$, AR), Ethanol absolute (C_2H_6O, AR) was obtained from Shanghai Aladdin Biochemical Technology Co., Ltd. CO_2 gas (99.999%) was purchased from Wuxi Xinxiyi Technology Co., Ltd. All chemical reagents were used as received without further purification.

1.3 Materials characterizations

X-ray diffraction (XRD) patterns were taken via a D8 X-ray diffractometer with Cu Kα radiation ($\lambda = 0.15406$ nm) in the 2θ range of 10~100° at the scanning rate of 5° min^{-1}, with the Cu Kα source operating at 40 kV and 20 mA. X-ray photoelectron spectroscopy (XPS) measurements were carried out with a AXIS Supra by Kratos Analytical Inc. All spectrums were calibrated by C1s (284.8 eV). Scanning electron microscopy (SEM) was carried out on a Hitachi S-4800 scanning electron microscope. Transmission electron microscopy (TEM) was conducted on a JEOL 2010 transmission electron microscope at 200 keV. Bright field and high-angle annular dark field scanning transmission electron microscopy (STEM) images, energy dispersive X-ray spectroscopy (EDS) mapping images were characterized by a FEI Tecnai F30 at an acceleration voltage of 300 kV. The infrared spectra (IR) were obtained on a Nicolet FT-IR 6700 spectrometer. The UV-visible spectrum was recorded on a TU-1901 spectrometer with a DH-2000 deuterium and tungsten–halogen light source in the absorbance mode (Beijing Purkinje General Instrument Co., Ltd, China). ATR-SEIRAS in situ testing was performed using an INVENIOR FT-IR (Bruker) spectrometer equipped with an MCT detector.

1.4 Detection of urea production

The diacetylmonoxime method was used to determine the concentration of urea. A series of standard urea solutions (0, 1, 2, 3, 4 and 5 ppm) were prepared. 10 mL of concentrated phosphoric acid and 30 mL of concentrated sulfuric acid were added to 60 mL of distilled water, mixed, and 10 mg of $FeCl_3$ was added to obtain solution A. Then 250 mg of diacetylmonoxime (DAMO) and 5 mg of thiourea (TSC) were dissolved in 50 mL of distilled water to obtain solution B. 2 mL of solution A and 1 mL of solution B were added to 1 mL of electrolyte drawn from the cathode chamber (or 1 mL of standard urea solution) and mixed well. The solution was then heated to 90 °C and held for 40 min. after cooling to 25 °C, the absorbance was obtained at 525 nm.

Urea yield equation:

$$R(urea)(mmol \cdot g^{-1} \cdot h^{-1}) \ = \frac{C(urea)(\mu g \cdot mL^{-1}) \times V(mL) \times 10^{-3}}{m(mg) \times 10^{-3} \times 60.06 \times t(h)} \qquad (7)$$

where R (urea) denotes the urea yield; C (urea) is the measured mass concentration of urea; V is the volume of the electrolyte solution; t denotes the reaction time; m is the mass of the catalyst.

The equation of Faradic efficiency:

$$FE \text{（urea）}\% = \frac{16 \times C(urea)(\mu g \cdot mL^{-1}) \times V(mL) \times 10^{-6} \times F}{60.06 \times Q} \times 100\% \qquad (8)$$

where C (urea) is the measured mass concentration of urea; V is the volume of the electrolyte solution; F denotes Faraday's constant (96485.34), and Q is the total amount of electricity applied.

1.5 Determination of CO and H_2

The gas product is quantified on a gas chromatograph connected to the headspace of the electrolytic cell. The thermal conductivity detector (TCD) is used to quantify H_2, and the flame ionization detector (FID) equipped with methanation tower is used to quantify CO. The Faraday efficiency of gas products is calculated according to the following formula.

$$FE = \frac{N \times P \times C \times g \times F}{R \times T \times i} \qquad (9)$$

where N denotes the number of electrons transferred (N = 2); P = 101,325 Pa; C is the concentration

of CO or H_2 detected by the GC; g (mL·min^{-1}) denotes the flow rate of the gas; F = 96,485 C. mol-1; R is the gas constant, R = 8.314 J·mol^{-1}·K^{-1}; T = 298.15 K; and i is the measured during the gas collection period Total current.

1.6 Determination of NH_3 concentration

The concentration of ammonia was determined using the indophenol blue method. First, the color developers (A) sodium hydroxide solution (containing 5 wt% salicylate and 5 wt% sodium citrate), (B) 0.05 M sodium hypochlorite solution, and (C) 1 wt% sodium nitroferricyanide (Na_2 [Fe(CN)$_5$NO]·$2H_2O$) aqueous solution were prepared, and sequentially, 2 mL of A solution, 1 mL of B solution, and 0.2 mL of the solution were added to 2 mL of electrolyte obtained from the cathode chamber, mixed well, and placed in a dark environment to react for 2 h. Finally, the absorbance was measured at 662 nm. The ammonia concentration was calculated using the calibration curve obtained. Calculate the rate of formation of NH_3 using the following equation:

$$R_{NH_3} = \frac{C_{NH_3} \times V}{t \times m} \qquad (10)$$

where C is the measured concentration of NH_3 (µg·mL^{-1}), V is the total volume of cathode electrolyte (mL), t is the time (h), and m is the catalyst loaded metal. The Faraday efficiency of NH_3 was calculated using the following equation:

$$FE_{NH_3} = \frac{8 \times F \times C_{NH_3} \times V}{17 \times Q} \qquad (11)$$

where F is the Faraday constant (96485 C mol^{-1}) and Q is the charge (C).

1.7 Determination of NO_2^- concentration

2 g of p-aminobenzenesulfonamide was added to a mixed solution of 25 mL of water and 5 mL of phosphoric acid, and 1 g of N-(1-naphthyl)-ethylenediamine dihydrochloride was dissolved in the above solution. The above solution was transferred to a 50 mL volumetric flask and diluted to scale, i.e., the color developer solution. For testing, the pH of the electrolyte was adjusted to weak acidity

with a saturated solution of boric acid. 1 mL of electrolyte was removed from the electrolyzer and diluted to 5 mL with 1 mL of H_2O and 3 mL of boric acid saturated solution.0.1 mL of color developer was added and allowed to stand for 15 min.Absorbance measurements were then taken at 540 nm. The NO_2^- concentration was calculated using the obtained calibration curve.

Calculate the rate of NO_2^- formation using the following equation:

$$R_{NO_2^-} = \frac{C_{NO_2^-} \times V}{t \times m} \qquad (12)$$

where c is the measured concentration of NO2- (μ g mL^{-1}), v is the total volume of cathode electrolyte (ml), t is time (h), and m is the metal supported by the catalyst. The Faraday efficiency of NO^{2-} is calculated using the following equation:

$$FE_{NO_2^-} = \frac{2 \times F \times C_{NO_2^-} \times V}{46 \times Q} \qquad (13)$$

where F is the Faraday constant (96485 C mol^{-1}) and Q is the charge (C).

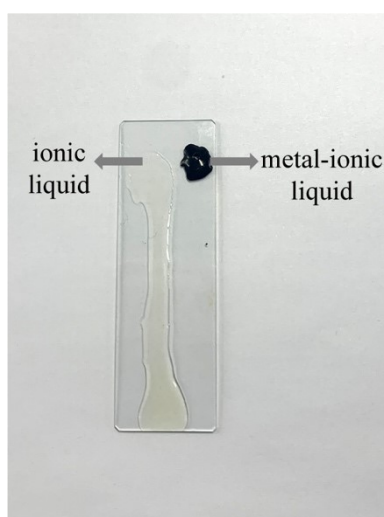## 2. Figures and Tables

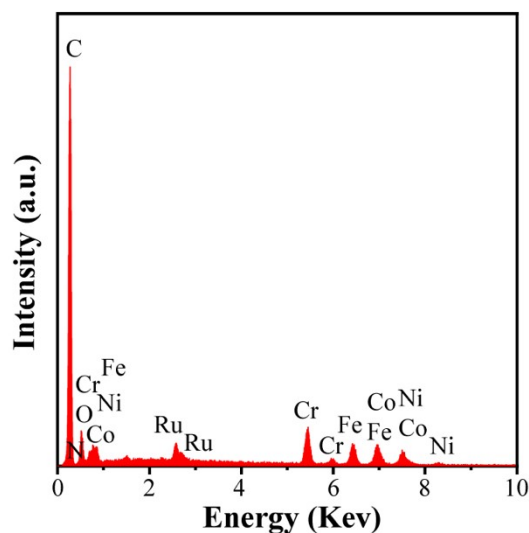**Fig. s1** Optical photograph of ionic liquid (left) and metal-ionic liquid (right)

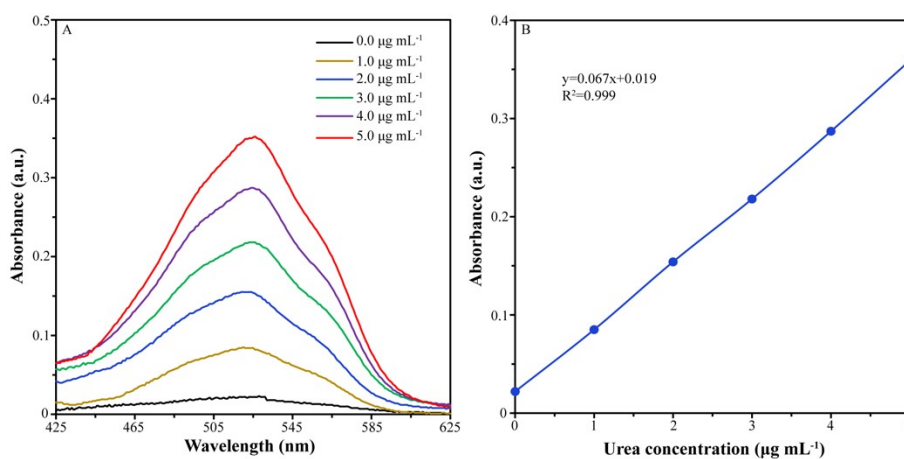**Fig. s2** EDS spectrum of CrFeCoNiRu$_{0.5}$-HENA/C

Fig. s3 (A) UV-Vis curves of diacetyl monoxime assays with different urea concentrations after heating at 90 ℃ for 40

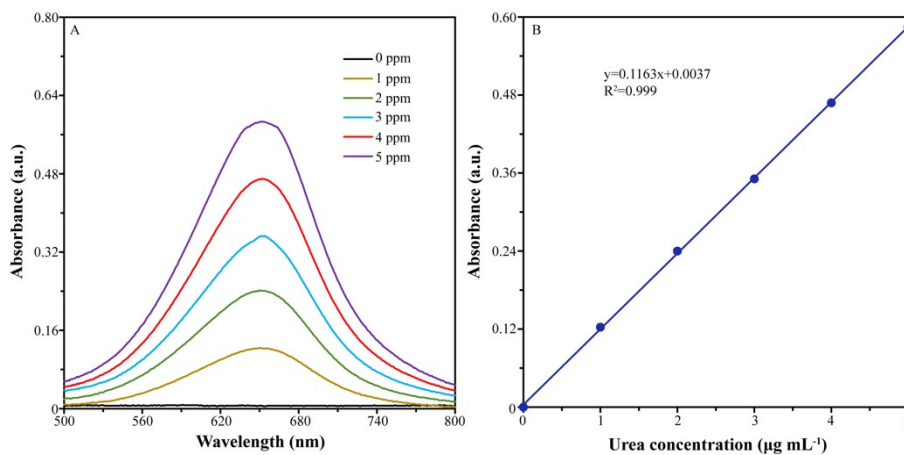min. (B) The calibration curve for urea quantification with a good linear relation (y=0.067x+0.019, R^2=0.999)

Fig. s4 (A) Absorption spectra of various NH$_3$ concentrations for three repeated experiments. (B) Calibration curve used

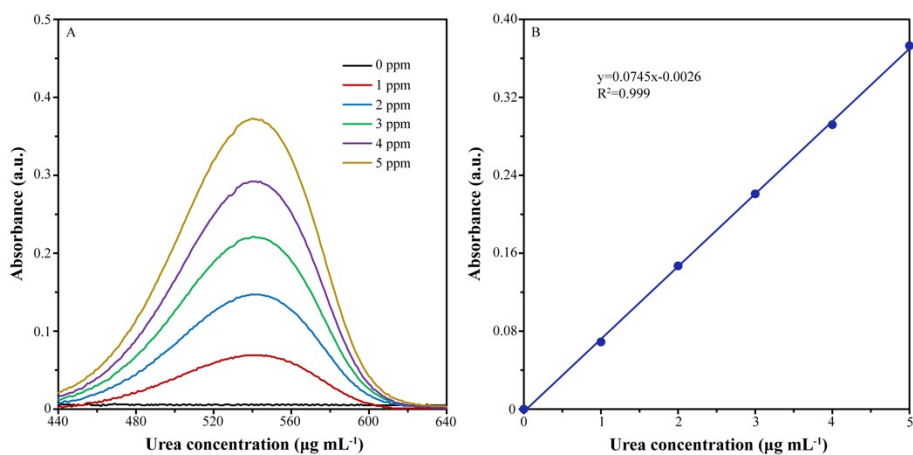for estimation of NH$_3$ concentration (y=0.1163x+0.0037, R^2=0.999).

Fig. s5 (A) Absorption spectra of various NO_2^- concentrations for three repeated experiments. (B) Calibration curve

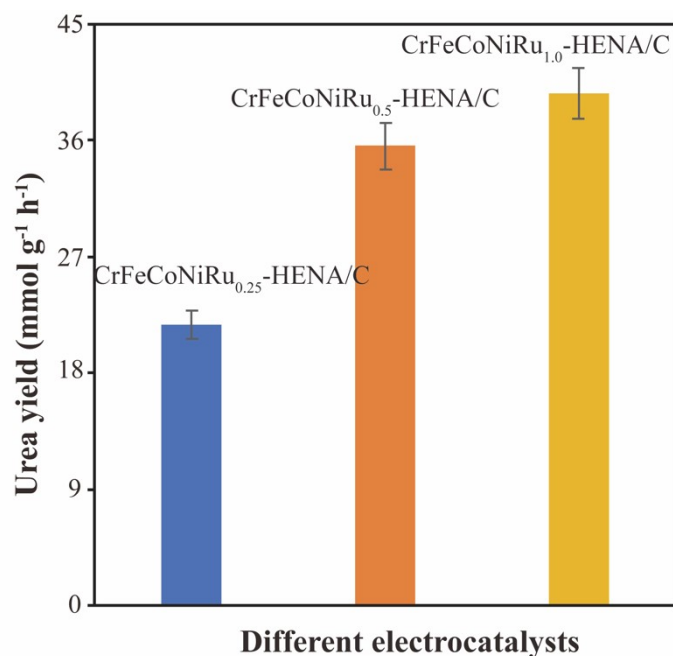used for estimation of NO_2^- concentration (y=0.0745x+0.0026, R^2=0.999).

Fig. s6 Urea yields of CrFeCoNiRu$_{0.25}$-HENA/C, CrFeCoNiRu$_{0.5}$-HENA/C and CrFeCoNiRu$_{1.0}$-HENA/C electrodes in the CO$_2$-

saturated 0.1 M KNO$_3$ electrolyte at -0.6 V for 60 min

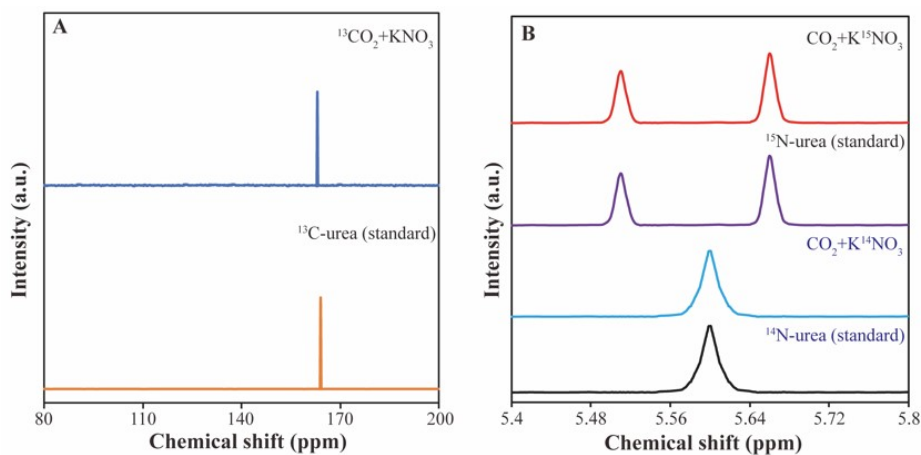**Fig. s7** ^{13}C NMR spectra of standard ^{13}C-urea and the solution electrolyzed by $^{13}CO_2+KNO_3$ saturated electrolyte at the potential of -0.6 V, and ^{1}H NMR spectra of standard ^{14}N-urea/^{15}N-urea and the solution electrolyzed by $CO_2+K^{15}NO_3/CO_2+K^{14}NO_3$ saturated electrolyte at the potential of -0.6 V for 2 h

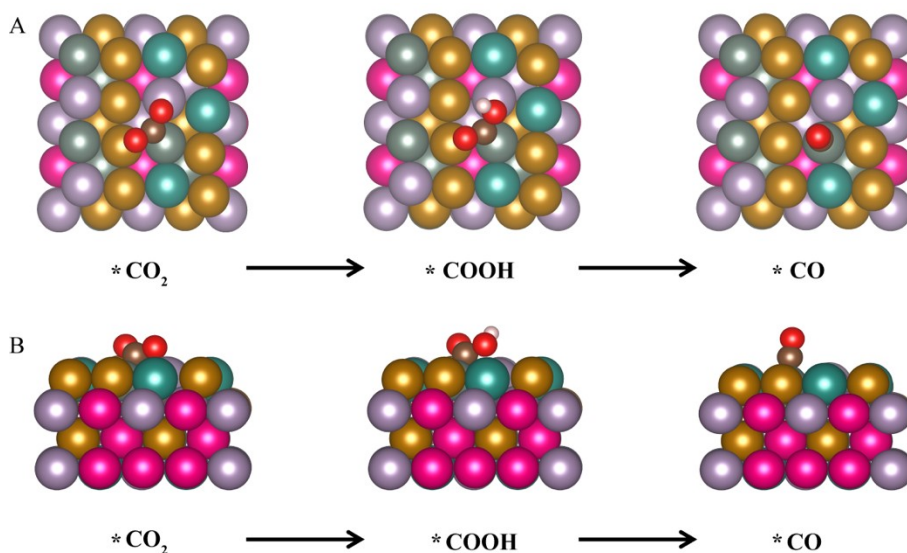**Fig. s8** Structure diagrams of CO_2 reduction process on $CrFeCoNiRu_{0.5}$. (A) Top view of $*CO_2$, $*COOH$ and $*CO$ on $CrFeCoNiRu_{0.5}$. (B) Side view of $*CO_2$, $*COOH$ and $*CO$ on $CrFeCoNiRu_{0.5}$. The meanings of the colored balls: Cr (purple), Fe (yellow), Co (grayish green), Ni (rose red), Ru (green), C (brown), H (pink), O (red), N (blue).

Fig. s9 Structure diagrams of nitrate reduction process on CrFeCoNiRu$_{0.5}$. (A) Top view of *NO$_3$, *NO$_2$, *NO$_2$H, *NO,

*NHO, *NHOH, *NH and *NH$_2$ on CrFeCoNiRu$_{0.5}$. (B) Side view of *NO$_3$, *NO$_2$, *NO$_2$H, *NO, *NHO, *NHOH, *NH

and *NH$_2$ on CrFeCoNiRu$_{0.5}$.The meanings of the colored balls: Cr (purple), Fe (yellow), Co (grayish green), Ni (rose
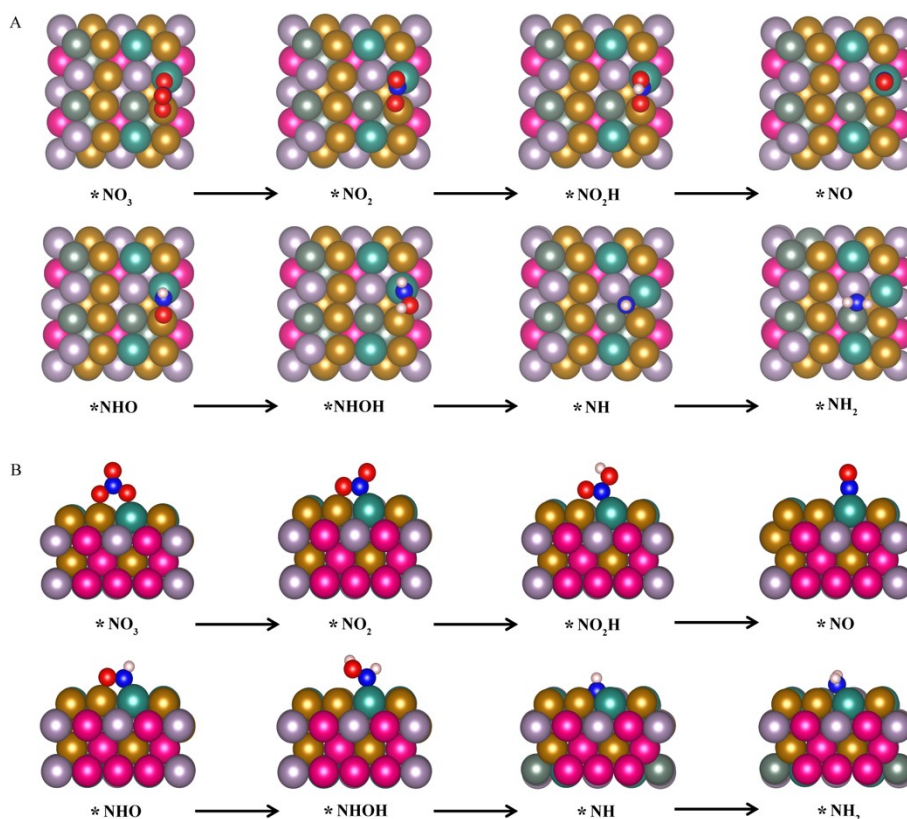
red), Ru (green), C (brown), H (pink), O (red), N (blue).

Fig. s10 Structure diagrams of C-N coupling reaction, on CrFeCoNiRu$_{0.5}$. Top view (A) and side view (B) of *CO+*NH$_2$,

TS and *CONH$_2$ on CrFeCoNiRu$_{0.5}$. The meanings of the colored balls:Cr (purple), Fe (yellow), Co (grayish green), Ni

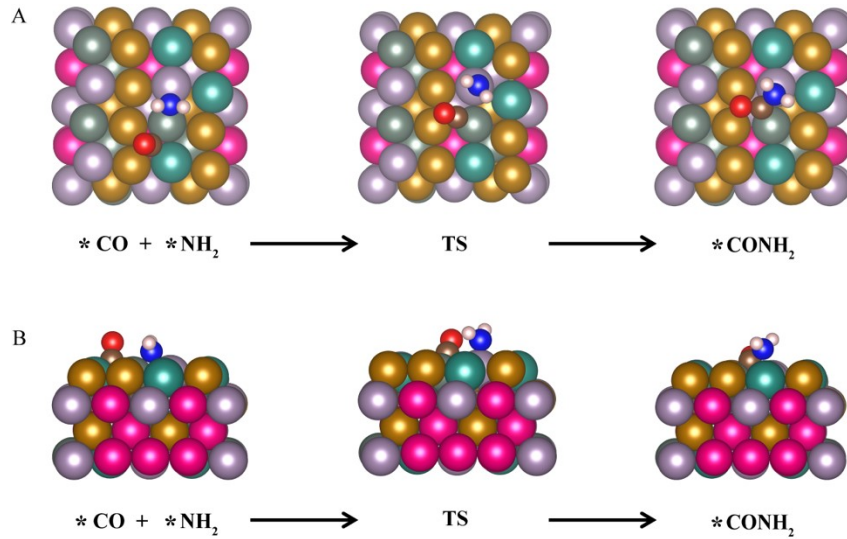(rose red),, Ru (green), C (brown), H (pink), O (red), N (blue)

Table s1 Binary mixing enthalpies (kJ mol^{-1}) and physico-chemical parameters of CrFeCoNiRu$_{0.5}$ [2]

Element	Ru	Fe	Co	Ni	Cr
Melting point /°C	2250	1538	1495	1455	1857
Atomic radius /pm	133	124	125	125	128
Valence electron concentration	8	8	9	10	6
Ru	0	-5	-1	0	-12
Fe		0	-1	-2	-1
Co			0	0	-4
Ni				0	-7
Cr					0

Table s2 Calculated thermodynamic and geometric parameters of CrFeCoNiRu$_{0.5}$

HEA	ΔSmix	ΔHmix	δ	Ω	VEC

	/J K mol^{-1}	/kJ mol^{-1}	/%		
CrFeCoNiRu$_{0.5}$	13.14	-4.74	2.18	5.36	8.22

Table s3 The atomic percentage of Fe, Co, Ni, Cr, Ru, C, N, O in CrFeCoNiRu$_{0.5}$-HENA/C measured by EDS

CrFeCoNiRu$_{0.5}$-HENA/C	C	N	O	Cr	Fe	Co	Ni	Ru
Atomic percentage (at. %)	82.21	2.71	10.25	1.04	1.11	1.08	1.06	0.54

3. References

[1] Byungchul Kang , Junho Lee , Ho Jin Ryu , Soon Hyung Hong. Ultra-high strength WNbMoTaV high-entropy alloys with fine grain structure fabricated by powder metallurgical process. Materials Science Engineering: A, 2018, 712, 616-624. Mater. Sci. Eng. 712 (2018) 616-624. https://doi.org/10.1016/j.msea.2017.12.021Get rights and content.

[2] A. Takeuchi, A. Inoue. Classification of bulk metallic glasses by atomic size difference, heat of mixing and period of constituent elements and its application to characterization of the main alloying element. Materials Transactions. 2005, 46(12), 2817-2829. Mater. Trans. 46 (2005) 2817-282 9. https://doi.org/10.2320/matertrans.46.2817.

[3] B. Chen, X. M. Li, Y. Y. Niu, R. Yang, W. J. Chen, B. Yusupu, L. Jia. A dual-phase CrFeNbTiMo refractory high entropy alloy with excellent hardness and strength. Materials Letters, 2023, 337,133958. Mater. Lett. 337 (2023) 133958-133961. https://doi.org/10.1016/j.matlet.2023.133958.

[4] Y. Zhang, Y. J. Zhou, J. P. Lin, G. L. Chen, P. K. Liaw. Solid-Solution Phase Formation Rules for Multi-component Alloys. Advanced Engineering Materials, 2008, 10(6), 534-548. Adv. Eng. Mater. 10 (2008) 534-548, https://doi.org/10.1002/adem.200700240.

[5] Y. Zhang , Z. P. Lu , S. G. Ma , P. K. Liaw , Z. Tang , Y. Q. Cheng , M. C. Gao. Guidelines in predicting phase formation of high-entropy alloys. Mrs Communications, 2014, 4(2), 57-62. MRS Commun. 4 (2014) 57-62, https:// doi.org/10.1557/mrc.2014.11.

[6] S. Guo, C. T. Liu. Phase stability in high entropy alloys: formation of solid-solution phase or amorphous phase. Progress in Natural Science: Materials International, 2011. 21(6): p. 433-446. Prog. Nat. Sci.:Mater. Int. 21 (2011) 433-446, https://doi.org/10.1016/S1002-0071(12)60080-X.

[7] S. Guo, C. Ng, J. Lu, C. T. Liu. Effect of valence electron concentration on stability of fcc or bcc phase in high entropy alloys. Journal of applied physics, 2011. 109(10), 103505. J. Appl. Phys. 109

(2011) 103505-103509, https://doi.org/10.1063/1.3587228.

[8] Z. J. Cao, K. T. Zhu, Y. Q. Yang, P. W. Xu, R. Y. Li, G. L.Wang, Z. J. Li, X. H. Liu. Ta_2O_5-graphene Schottky heterojunction composite symmetric upercapacitor with ultrahigh energy density for self-powered pulse sensor dri- ven by green long afterglow phosphor-enhanced solar cell. Applied Surface Science (Appl. Surf. Sci.) 605 (2022)154730-154744. https://doi.org/10.1016/j.apsusc.2022.154730.